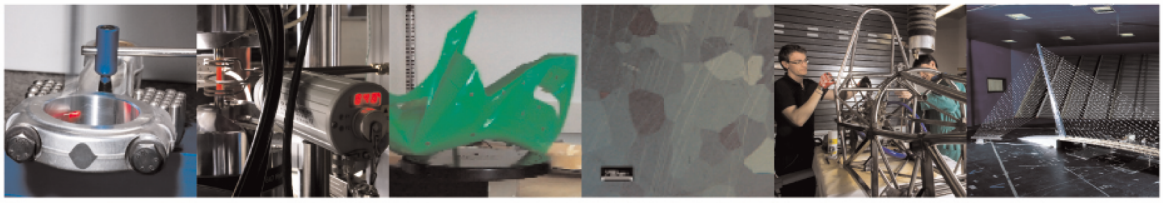
POLITECNICO
MILANO 1863

DIPARTIMENTO DI MECCANICA

mecc



3D Modelling of the Deposit Profile in Cold Spray Additive Manufacturing

Vanerio D.;Kondas J.;Guagliano M.;Bagherifard S.

This is a post-peer-review, pre-copyedit version of an article published in Journal of Manufacturing Processes. The final authenticated version is available online at: https://doi.org/10.1016/j.jmapro.2021.05.013

© <2021>

This content is provided under CC BY-NC-ND 4.0 license

3D Modelling of the Deposit Profile in Cold Spray Additive Manufacturing

Daniele Vanerio[1], Jan Kondas[1,2], Mario Guagliano[1], Sara Bagherifard[1]

[1]Department of Mechanical Engineering, Politecnico di Milano, Milan, Italy
[2]Impact Innovations GmbH, Bürgermeister-Steinberger-Ring 1, 84431 Haun/Rattenkirchen, Germany

Abstract

New fields of application are coming along at an outstanding pace for cold spray deposition. More recently cold spray is being introduced as an additive manufacturing method that supersonically accelerates microparticles to induce bonding via severe plastic deformation. However, the thriving of cold spray as a widespread additive manufacturing technology with high production rates is still limited by inadequate geometrical control of the deposit shape. Thus, to establish cold spray as in the additive manufacturing sector, substantial development is still required regarding digitalization and automatization of the process. To take a further step towards gaining control on the deposit geometry, present study reports the development of a 3D model able to simulate the cold spray deposit profile. The physical basis of the model is represented by a partial differential equation, which describes the deposit profile evolution as the number of passes grow. The model offers total freedom regarding the choice of the nozzle trajectory and the substrate geometry. The effects of the various process parameters, namely the number of scanning passes, spray angle, scanning speed and stand-off distance are implemented and realistically reflected in the model. More complex conditions like superimposed tracks with different spray angles, curved substrates, shadow effect and non-Gaussian profiles have been effectively simulated. The developed model has been validated with a wide range of experiments, demonstrating high accuracy and notable potential to promote the digitalization of cold spray additive manufacturing.

Keywords: Cold gas dynamic spray**,** supersonic impact, 3D printing**,** simulation**,** deposit shape

1. Introduction

Cold Spray (CS) is an emerging deposition technology in which a supersonic jet of gas accelerates powder particles, with typical diameter of 20-60 μm. The accelerated particles impact the substrate at velocities usually ranging between 300 and 1200 m/s. The compressed gas is typically accelerated using a convergent-divergent De Laval nozzle [1–4]. If the particles are accelerated above the critical velocity [5], when impacting on the substrate, they adhere to it, progressively forming a dense deposit. The critical velocity is known to be a function of material's thermo-mechanical properties [6]. The characteristic low working temperature has established CS as an efficient coating and repair technology for various fields of application [7–9]. More recently, however, CS has been evaluated as an additive manufacturing (AM) technique to create freeform components, also for load bearing applications [3, 10]. The interest in cold spray additive manufacturing (CSAM) is coherent with the global scenario of developing high-performance metal AM, pushed by the unique advantages of this family of processes over traditional manufacturing techniques [11]. In the past few years the boundaries of CSAM have been pushed by depositing not only simple geometries of small size but also thick components and complex, topologically optimized and almost net shape parts [3, 12, 13].

Most widespread metal AM technologies can be classified into two broad groups of powder bed fusion (PBF) and direct energy deposition (DED) systems [14], both involving melting of the feedstock material. The melting and re-solidification can bring in detrimental effects for material properties as oxidation, phase transformation, grain growth and undesired thermal residual stresses [11]. In CSAM instead, the powder is not significantly heated and bonding occurs in solid state; thus, deposits with very low oxide contents can be produced, feedstock phase composition and microstructure are prevalently preserved and compressive residual stresses are generated within the deposit, leading to positive effects on the mechanical behavior of the deposited material [3, 15, 16]. Furthermore, temperature-sensitive, oxygen-sensitive and high-reflectivity materials such as copper, which are difficult to process with commonly used AM techniques, can be easily handled in CSAM; last but not least, the notably higher deposition rate of CSAM differentiates it from all other available metal AM technologies [17, 18].

Despite these advantages, the main aspects that impede the establishment of CSAM, are its limits in deposit resolution and geometrical accuracy. Geometrical control of as-fabricated components is actually a common problem also in high production rate AM techniques such as wire arc additive manufacturing (WAAM) [19, 20] and some other DED systems [21, 22]. Addressing this issue is of major importance for the

development of high speed AM processes, to avoid or reduce the necessity for post-machining operations, ensure a consistent quality and facilitate the fabrication of complex shapes [3, 23].

In the case of CSAM, an accurate geometrical control, that is not fully matured yet, is necessary for further development of this technology and to boost its wide recognition as an efficient AM process [23]. Despite being a key factor in industrialization and commercialization of CSAM [3, 23], insufficient data are available about the evolution of deposit shape and the very few presented simulation approaches, despite shedding light on many new aspects, are still limited in replicating complex toolpaths and complex geometries.

The shape of the deposit in CSAM is strictly linked to multiple process parameters and the accurate definition of their relationship is still a matter of research. In the recent years, there has been some advancement in the simulation of the elementary unit, i.e. the single track, to evaluate the effect of process parameters on deposit thickness uniformity and profile shape through superimposition principle [24–26]. A model for the prediction of the deposit profile has been implemented in the Profilekit module of Thermal Spray Toolkit (TST) add-in software. This 3D geometric profile simulation (initially developed in 2D) can predict coating thickness and shape in the case of complex curved substrates considering also shadow effect. Moreover, it presents many interesting features, e.g. the possibility to introduce the substrate as a CAD file to be integrated with a robotic off-line programming software for the generation of trajectories. The effect of different parameters including spray angle, spray distance and transverse speed are implemented into this model [23]. However, as pointed out by Klinkov at al. [27], the approach implemented in this software is not physically justified and it cannot simulate the profile evolution as the number of passes increases. The original 2D version of the TST software was employed by Cai et al. [26] to study the effect of spray distance and scanning step on coating thickness uniformity. The 3D model was instead used by Wu et al. [28] to obtain a qualitative profile prediction for the implementation of a spray strategy able to generate a vertical wall. Ikeuchi et al. [23] developed an artificial neural network (ANN) to simulate the track profile of CSAM in 2D. The ANN approach has proven to be able to simulate the effects of spray angle, transverse speed and standoff distance with an accuracy comparable to the Profilekit module of the TST software, while improving estimations at the profile extremities. However, due to the inherent nature of ANN algorithm, this model requires a massive quantity of experimental data to be able to provide accurate results. Another interesting model developed by Jeandin et al. [29] considers the one-pass deposits profile as the initial input to the program and also reflects the effect of impact angle on deposition efficiency. The most attractive feature of this model is the analysis and implementation of some particular aspects such as the direction reversal of the nozzle scan track and the deposit profile roughness. This model is developed in 2D and its pseudo-3D extension is simply a projection of the 2D profile.

Klinkov et al. developed a 3D simulation with strong physical basis and with the ability to describe the evolution of the profile shape during deposition [30]. In spite of the fact that it has not been experimentally validated, Klinkov model can be recognized as one of the most robust models currently available for the description of CS deposit profile. The model, indeed, is based on input data which are easily observable and measurable for any material and spray condition. Moreover, being based on the fitting of different profiles for the identification of the best fitting parameters, the approach suggested by Klinkov et al. strongly reduces the effect of stochastic events. However, notwithstanding the valid principles, Klinkov model's application is limited, mainly regarding the range of substrate geometries. Since it defines the substrate based on a grid laying on the xy-plane, a visible distortion from real profile is observed when using this model for non-planar substrates. Moreover, this approach models the thickness increment to occur along the out of plane (z) direction, thus it cannot be used to generate more complicated features like vertical walls and overhangs, as they required more flexible deposition and buildup strategies.

To sum up, the available models have brought valuable insight to the modelling of CSAM profile; however, there are still multiple deficiencies that limit their applicability. To our best knowledge, all of the abovementioned models lack in comprehensive experimental validation. A viable example of the limitations is that the implementation of jet particle distribution profile is limited to the Gaussian shape in all models. When axisymmetric nozzles are used, the profile shape, for low number of layers and relatively high transverse speed of the nozzle, can be usually approximated with a Gaussian function that gradually evolves into a triangular-like profile, if lower speeds are used or the number of passes is increased [25, 27, 28, 31, 32]. In some cases, however, in practice non-Gaussian particle distributions can be observed; this could probably be attributed to the different particle velocity in the propelling gas stream; this could lead to the deposition of also larger powder particles that reach the critical velocity only in the middle of the propelling gas stream, while they are rebounded at the sides of the gas stream due to insufficient velocity. None of the existing models has been tested until now for the simulation of non-Gaussian deposit profiles.

Herein, a versatile model is proposed for the simulation of CS deposit profile. Founded on the same physical basis suggested by Klinkov et al. [30], the new model is defined in a way to address and overcome the existing limitations. This model is able to accurately simulate the 3D profile of the CSAM deposit and to describe its evolution in basic deposition conditions; moreover, it can simulate the shadow effect, the deposit profile shape and its development on non-planar substrates and the generation of superimposed tracks. Furthermore, this model incorporates the possibility of considering any nozzle axis orientation and thus offers significant flexibility for depositing complex geometries. In the following sections, the physical and mathematical principles of the model and its development steps are explained in detail, introducing all incorporated functions and features. In Table 1 the characteristics of the previous models and the model proposed in this work are schematically reported and compared. We have listed the major deficiencies of the previous models for predicting the 3D profile of the CS deposit. ANN [23] model is limited to 2D, does not have a physical basis and considers very restricted range of parameters regarding substrate geometry and superposition of tracks. TST [28], on the other hand, does not have strong physical basis, thus it cannot describe the profile evolution and has not been validated using very limited experimental tests; it also does not incorporate non-Gaussian distributions for the powder jet. Klinkov model [30], instead, is able to correctly describe the profile evolution; however, it has limited application range and has not been experimentally validated. Table 1, which provides a detailed comparison between the capacities and shortcomings of all the available models, depicts the novelty of the new model proposed in this paper. This new model integrates all the positive characteristics of the previous models in a unique solution that is validated using an extensive experimental campaign; moreover, it is the first model to incorporate non-Gaussian distributions for powder jet, thus offering a more notable flexibility and wider range of application.

Table 1 – Comparison of the new model with the available models for CS profile prediction

	TST [28]	**ANN** [23]	**Klinkov** [30]	**New model**
3D	✓	✗	✓	✓
Physical basis	✗	✗	✓	✓
Profile evolution	✗	✓	✓	✓
Shadow effect	✓	✗	✗	✓
Non-planar substrates	✓	✗	✗	✓
Data-driven approach	✗	✓	✗	✗
Mathematical approach	✓	✗	✓	✓
Superimposed tracks	✓	✗	✗	✓
Experimental validation	limited	limited	✗	✓
Non-Gaussian distribution	✗	✗	✗	✓

A series of experimental tests were developed to validate the suggested model using Ti6Al4V and Al2024 deposits. To highlight the flexibility of the model, its predicted profile shapes were also compared with experimental data available in the literature for pure Cu, Al5056 and Al7075 deposits. The model was used to track the evolution of deposit profiles upon variation of multiple process parameters. The obtained modelling and experimental results are critically discussed, highlighting the strengths and the limits of the suggested model.

2. Methods, experiments and materials

2.1 Principles of the Klinkov model

The physical concepts defining the model suggested by Klinkov et al. [30] were used as the basis of the model developed in this work. Therefore, here the main hypotheses of Klinkov model are briefly described:

- Deposition efficiency (DE) is experimentally defined as a function of the impact angle α.
- The particles are assumed to fly parallel to the nozzle axis.
- Jet particle's distribution profile $J(r)$, i.e. the profile of the particles coming out from the nozzle, is approximated with an axisymmetric function, that is considered to be Gaussian-based:

$$J(r) = \begin{cases} \dfrac{e^{-k_2(r/r_n)^2} - e^{-k_2}}{1 - e^{-k_2}} & r < r_n \\ 0 & otherwise \end{cases} \qquad 1$$

The parameters r_n and k_2 are parameters obtained by fitting the experimental data and r is the distance from the nozzle axis.

2.2 New model description

The new model is based on the same hypotheses of Klinkov model excluding the last one. In the present model, in fact, the jet particle's distribution profile is axisymmetric, but not necessarily Gaussian-based, as better explained in Paragraph 3.5. The present model tackles the limitations associated with the definition of substrate as an xy-plane grid and thus it is able to incorporate an unlimited range for substrate geometries. Fig. 1 presents a flowchart summarizing the modeling steps. To offer more flexibility, the substrate geometry can be introduced as a CAD file in stereolithography (STL) format; the same file format is obtained also for the output of the simulation. The STL files contain information about a surface mesh consisting of a list of triangles. Each triangle is identified by twelve floating point numbers, three for the surface normal and three for the xyz coordinates of each vertex. The choice of STL format, however, implies that the substrate mesh characteristics will strongly depend on the process used by the CAD software to generate the input file. To guarantee the accuracy of the results a homogeneous mesh with a pre-set maximum element size, identified through trial and error process, was considered. This remeshing process was implemented in two different steps. First, the mesh obtained from the CAD model conversion to STL file was refined. Then, during the simulation, a second remeshing step was implemented between subsequent passes, when the maximum element size limit was exceeded, to avoid elongation of triangular faces and numerical errors. An example of remeshing on a planar substrate can be observed in Fig. 2b.

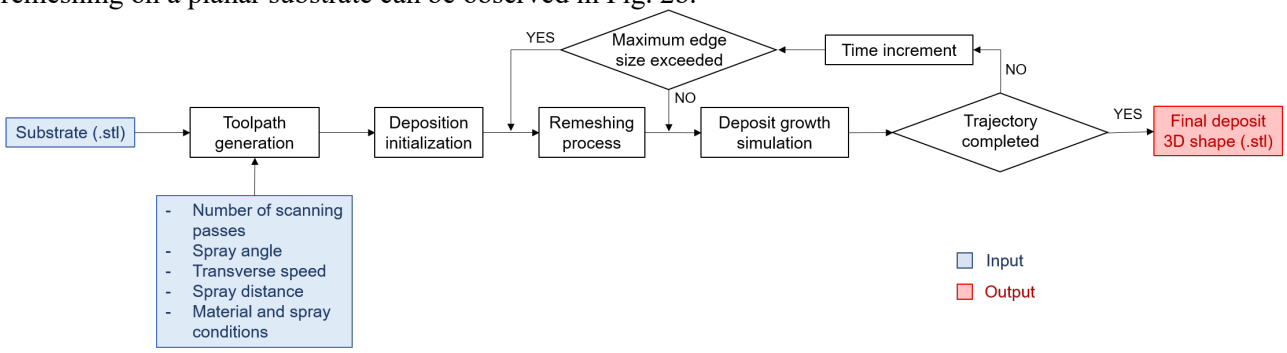


Figure 1 - Flowchart summarizing the modelling steps

Being independent from the coordinate system, the new model also allows considering any trajectory for the nozzle. The Klinkov et al. [30] model indicated the nozzle position by defining the intersection point of the nozzle axis and the planar substrate. Here we improved the model by defining the coordinates of the nozzle position. To this end, a new nozzle trajectory was defined in which the nozzle position refers to the centre of the nozzle outlet section and is indicated by vector coordinates $\bar{v}_{nposition} = (x_n, y_n, z_n)$. Director cosines principle was used to generate the nozzle axis vector as $\overline{v_n} = (\cos(\beta_x), \cos(\beta_y), \cos(\beta_z))$. The convention used for the angles β_x, β_y and β_z is represented in Fig. 2a.

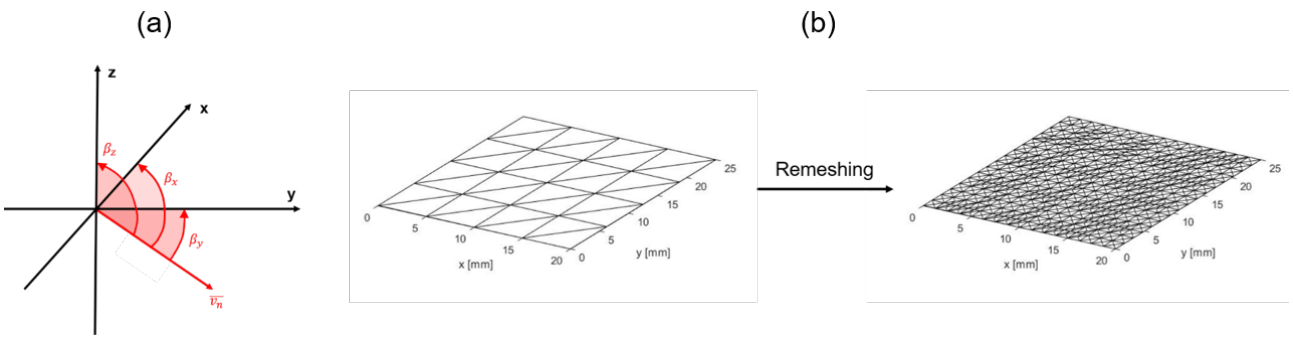


Figure 2 - (a) The convention used for nozzle vector definition (b) Remeshing of a planar substrate

After introducing the substrate geometry and generating the nozzle trajectory, the growth of deposit thickness is calculated for each element face. First, the vectors normal to triangular face of each element, $\overline{v_f}$, is defined. The impact angle α is then calculated as the angle between the normal vector of the triangular face and the nozzle axis vector, $\overline{v_n}$. $\mathrm{Tan}(\alpha)$ (α is the impact angle) is then calculated according to Eq. 2. To avoid bounding the deposit growth to z-axis direction, the profile growth is calculated along the direction of the nozzle axis and the mesh is modified, accordingly. The thickness increment for each vertex is obtained by averaging the increments calculated for all the faces to which the vertex belongs. The final equation to describe the thickness growth rate of the profile along the direction of the nozzle axis is described in Eq.3, where the experimentally estimated coefficient A, obtained by fitting the experimental data, represents the rate of increase of the deposit height. This coefficient depends on the sprayed material and spray parameters.

$$tan(\alpha) = \frac{\left\|\overline{v_f} \times \overline{v_n}\right\|}{\overline{v_f} \cdot \overline{v_n}} \qquad 2$$

$$\frac{\partial z_{axis}}{\partial t} = A \cdot DE(\tan(\alpha)) \cdot J(r) \qquad 3$$

The Eq. 3 is then solved numerically by using Method of lines (MOL) [33] to discretize the problem and by implementing Euler method [34] to each triangular face to compute the corresponding thickness increment.

In the following section different features implemented in the model to enhance its accuracy and amplify its applicability are described.

2.2.1 Spray distance effect

Changing the spray distance d_s, can influence both DE and the deposit profile shape for each material and spray conditions. To account for this effect, $DE_d(d_s)$ curves can be generated, based on experimental data for each material, and the function can be introduced into the deposit growth Eq. 4. Introducing this effect adds a new variable to the jet particle's distribution profile, $J(r) \rightarrow J(r, d_s)$.

$$\frac{\partial z_{axis}}{\partial t} = A \cdot DE_\alpha(\tan(\alpha)) \cdot DE_d(d_s) \cdot J(r, d_s) \qquad 4$$

To mimic the effect of spray distance on deposit shape, the starting particle's distribution profile function was stretched and scaled, maintaining the same volume obtained by rotating $J(r)$ function around the nozzle axis, thus retaining the same mass of sprayed material. Mathematical representation of the stretching process is shown in Eq. 5, where c_{st} represents the stretching coefficient. The scaling process is instead described by Eq. 6, where the left side term corresponds to the volume obtained by rotating the initial curve around the nozzle axis, and the right side term corresponds to the same volume in the case of the final curve; c_{sc} represents the scaling coefficient.

$$f(x) \rightarrow f(c_{st}x) \qquad 5$$

$$2\pi \int_0^{r_n} x f(x)\, dx = 2\pi c_{sc} \int_0^{r_n} x f(c_{st}x)\, dx \qquad 6$$

2.3 Shadow effect

Shadow effect was considered to model cases in which some regions of the substrate or of the already formed deposit, obstruct the particles' flight, generating a "shadow" region where no deposit can be formed. This phenomenon is represented in Fig. 3a, where it can be observed that in the shadow region (the grey area), no deposit formation occurs.

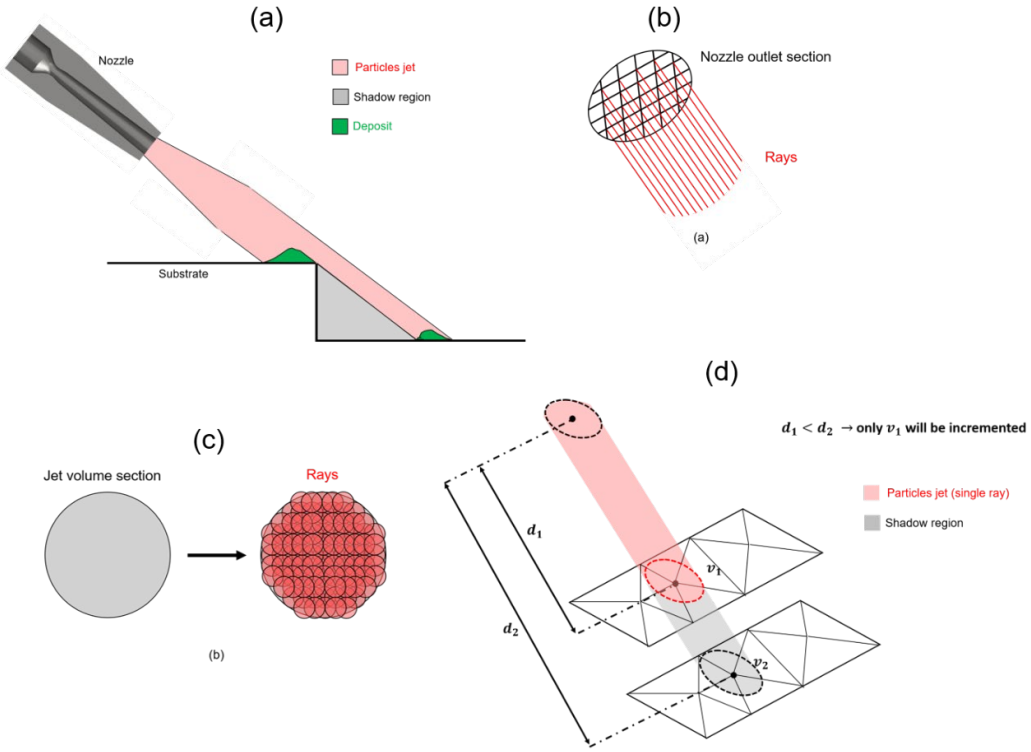


Figure 3 - Shadow effect (a) Phenomenon representation (b) Rays generation representation (c) Jet volume cross-section subdivision (d) Shadow region identification via determination of the closest vertex.<a

The shadow effect has already been successfully modelled by Wu et al. [24]. In their study the authors considered the particles as rays sharing the same starting point and identified the intersection of these rays with the substrate. The deposit was then generated starting from the identified intersection points. A similar principle was applied in the present study. A series of rays parallel to the nozzle axis were generated starting from the outlet section of the nozzle. At this section, a constant step grid was generated, and a ray started from each point of this grid, as represented in Fig.3 b. The rays then acted as axes to divide the jet volume into smaller cylindrical volumes (Fig. 3c).

Each cylindrical sub-volume could contain any number of vertices. The vertices contained in each sub-volume were identified and among them, the vertex which resulted to be the closest to the centre of the nozzle outlet section was spotted. The thickness increment was thus applied only to the faces to which this vertex belonged, since the faces identified by other vertices contained in the sub-volume were "hidden" by these ones as represented in Fig. 3d.

2.4 Experimental sample preparation

An experimental campaign was conducted to validate the developed physical model and to evaluate its deposit profile shapes predictions as a function of different spray parameters. Al2024 (Impact Innovations GmbH, Germany) and Ti6Al4V (AP&C, Canada) powder particles were used to deposits the samples using ISS 5/11 cold spray system (Impact Innovations GmbH, Germany). The powders' particle size distributions (PSD) are reported in Table 2.

Table 2 – Powder particle size distribution

Powder	D10 [µm]	D50 [µm]	D90 [µm]
Ti6Al4V	21	37	47
Al2024	39	55	76

In the case of single tracks, samples of 30 mm length were sprayed varying multiple process parameters. Samples' cross sections were embedded in resin, ground with subsequent graded SiC papers and finally polished with diamond suspension up to 1 µm. The polished cross sections were observed using Keyence VHX-5000 optical microscope and the profiles were obtained through image processing of the

obtained micrographs. First the micrographs were converted from RGB to B&W images, then the deposit border profile was identified with a developed MATLAB function.

The relevant spray parameters that were kept constant throughout the whole experimental campaign are listed in Table 3. The experimental campaign was planned to study the role of individual spray parameters including number of scanning passes, spray angle, scanning speed and spray distance on the track profile shape. The parameters that were varied for Al2024, Ti6Al4V and Cu deposits can be found in Table 4, Table 5 and Table 6, respectively.

Table 3 – CS parameters kept constant in all experiments for each material

Material	Powder feed rate [g/min]	Carrier gas	Gas temperature [°C]	Gas pressure [MPa]
Ti6Al4V	24.25	N_2	1100	5
Al2024	25.75	N_2	600	5
Cu [30]	24.00	Air	500	3

In the case of Ti6Al4V, a classical $J(r)$, defined as indicated in Eq. 1 was employed. Whereas the Al2024 profile shape deviated from the typical Gaussian distribution and was characterized by steeper extremities and two inflection points on each side of the peak (see Fig. 9). Thus, the corresponding distribution profile was implemented in the model for predicting the Al2024 deposit profiles, rather than using the typical Gaussian one.

The model was further validated also against some experimental profiles available in the literature for pure Cu [28], Al5056 [25] and Al7075 [24] for various deposition conditions. Pure Cu was a particularly interesting choice, since its deposit shape presents a more pronounced transition from Gaussian to triangular-like profile, when the effect of the number of scanning passes is analyzed.

To validate the efficiency of the model in the case of complex conditions, three specific case studies were considered as demonstrators for simulation and experimental validation using TiAl6V4 powder. The first demonstrator was to deposit superimposed tracks with different spray angles, whereas the second one dealt with depositing on a curved substrate, i.e. a section of a cylinder with 42 mm inner diameter, sprayed in the longitudinal direction. The last case study was to deposit material on a stepped-shape substrate representing the shadow effect.

Table 4 - CS parameters varied for Al2024 deposits

Sample type	Number of scanning passes	Spray angle [°]	Nozzle transverse speed [mm/s]	Spray distance [mm]
Number of scanning passes	15, 25	90	250	20
Spray angle	10	50, 60, 70, 80, 90	250	20
Nozzle transverse speed	10	90	125, 250, 500	20
Spray distance	10	90	250	10, 15, 20, 25, 30

Table 5 - CS parameters varied for Ti6Al4V deposits

Sample type	Number of scanning passes	Spray angle [°]	Nozzle transverse speed [mm/s]	Spray distance [mm]
Number of scanning passes	10, 14, 20	90	250	30
Spray angle	20	60, 70, 80, 90	250	30

Nozzle transverse speed	20	90	150, 250, 350	30
Spray distance	20	90	250	20, 25, 30, 35, 40
Superimposed tracks	20 (for each track)	90° 1st track 60° 2nd track	250	30
Curved substrate	20	90	250	30
Shadow effect	20	60	250	30

Table 6 - CS parameters varied for Cu deposits [28]

Sample type	**Number of scanning passes**	**Spray angle [°]**	**Nozzle transverse speed [mm/s]**	**Spray distance [mm]**
Number of scanning passes	1,3,7,9,15,20	90	100	30

3 Results and discussion

The profile shapes predicted by the model were compared with multiple experimentally achieved track profiles and their evolution as a function of different spray parameters, considering the typical Gaussian and also non-Gaussian deposit profiles. The obtained results for Ti6Al4V, Al2024 and Cu are reported in the present section, while the results for Al5056 and Al7075 can be found in the supplementary material, for the sake of brevity.

The simulation and experimental results were graphically compared, and the normalized root mean square error (RMSE) was calculated for each curve to quantify the accuracy of the simulation algorithm. The normalization was done dividing the RMSE by the profile average thickness.

3.1 The effect of number of scanning passes

When multiple scanning passes are applied on a single track, the initial profile, which typically has a smooth form, becomes sharper as the number of passes increases [28]. This shape variation cannot be simply simulated by superimposition of successive layers. The developed model offers the possibility to accurately simulate the growth and evolution of the profile as the number of passes increase; this capability, also introduced by Klinkov model [30], is derived from Eq. 3, which considers the contribution of the main process parameters. The results presented in Fig. 4a exhibit the excellent match between the experimental and numerical data for prediction of the Ti6Al4V deposit shape obtained from 10, 14 and 20 successive layers.

To further demonstrate the robustness of the developed model, the effect of number of passes was also simulated in the case of pure Cu, which exhibits a different profile shape variation trend compared to Ti6Al4V. As observed in Fig. 4b, unlike Ti6Al4V, Cu presents a very marked transition from Gaussian to triangular-like profile as the number of passes increase, probably due to its higher ductility compared with Ti6Al4V. The results, in this case were compared with the experimental data reported by Wu et al. [28], confirming a very close fit.

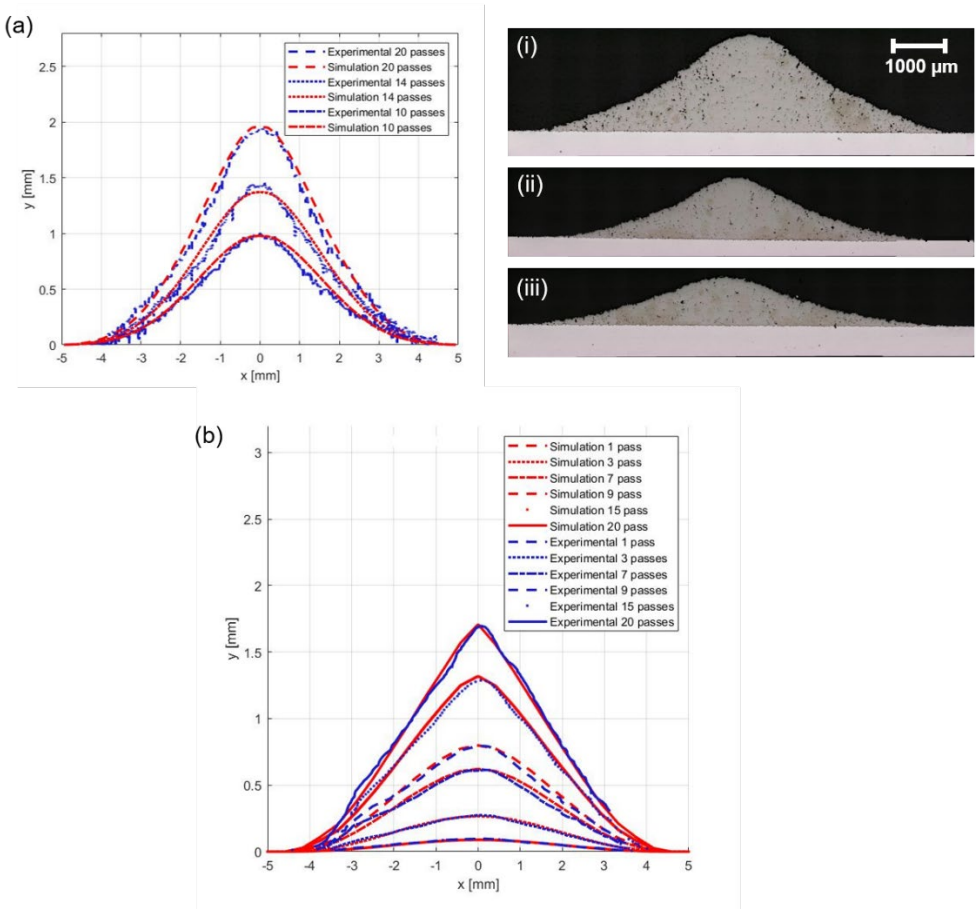


Figure 4 - The effect of number of scanning passes (a) Comparison of simulation results with the experimental profiles for Ti6Al4V deposits obtained for 10, 14 and 20 passes (i) Cross-section of Ti6Al4V deposit with 20 passes (ii) Cross section of Ti6Al4V deposit with 14 passes (iii) Cross section of Ti6Al4V deposit with 10 passes (b) Comparison of simulation results with experimental data for Cu deposits of up to 20 passes [28]

3.2 The effect of spray angle

The profile shapes obtained for Ti6Al4V under varied spray angles demonstrate in all cases a good estimation of the final thickness and shape of the deposit, as reported in Fig. 5. The deviation of the spray angle from normal direction, is found to strongly decrease the DE, as expected. At low spray angles, the considerable decrease of DE leads to deposit thickness reduction. Moreover, at reduced spray angles the deposit profile widens and the peak shifts from the centre [24, 25]. The predicted profiles evidence that the peak position displacement is well-captured by the simulation. Different views of the 3D simulated profiles are illustrated in Fig. 6.

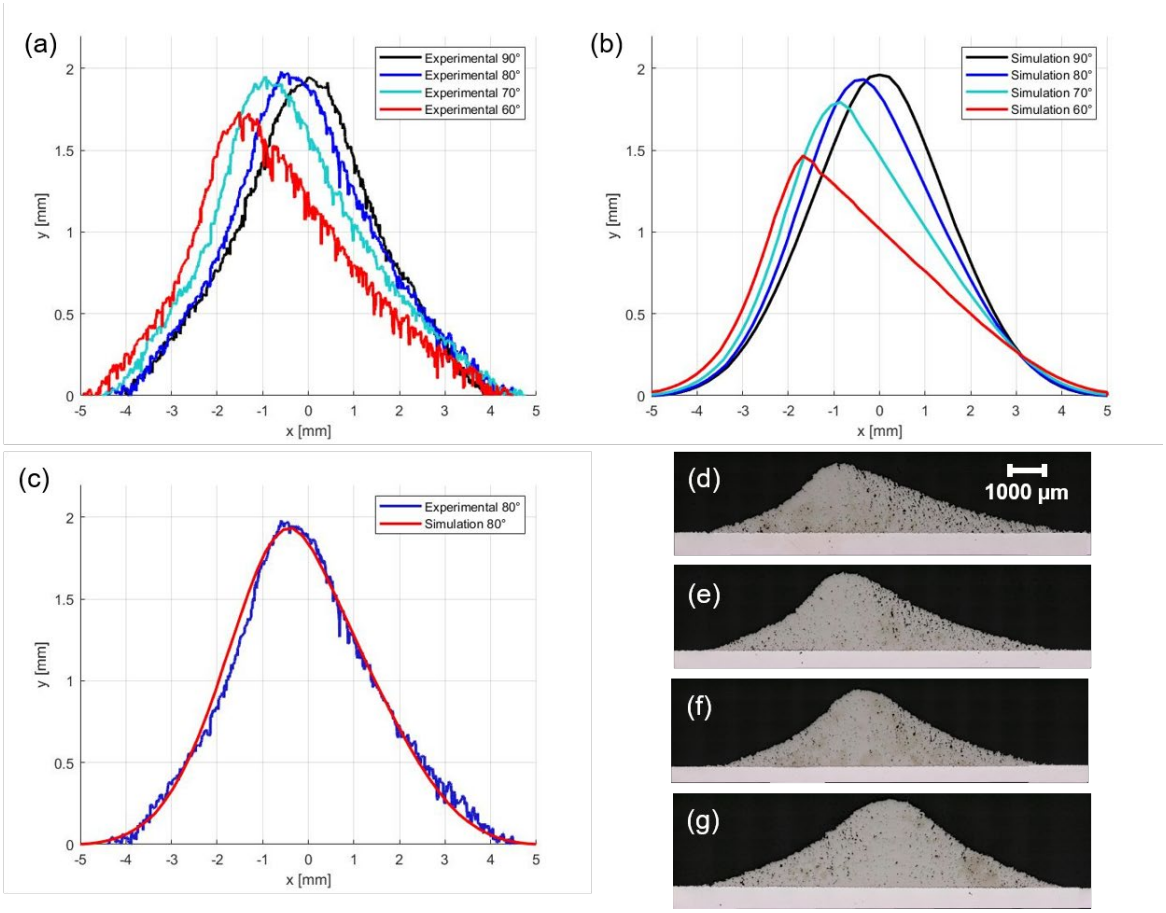


Figure 5 – The effect of spray angle on the shape of Ti6Al4V profiles obtained by 20 passes (a) Experimental results for spray angles varying from 90° to 60° (b) Simulation results for spray angles varying from 90° to 60° (c) Comparison of experimental profile with simulation for 80° spray angle as a representative profile among the predicted ones (d) Cross-section of Ti6Al4V deposits obtained by 20 passes at 60° spray angle (e) Cross-section of Ti6Al4V deposits obtained by 20 passes at 70° spray angle (f) Cross-section of Ti6Al4V deposits obtained by 20 passes at 80° spray angle. (g) Cross-section of Ti6Al4V deposits obtained by 20 passes at 90° spray angle

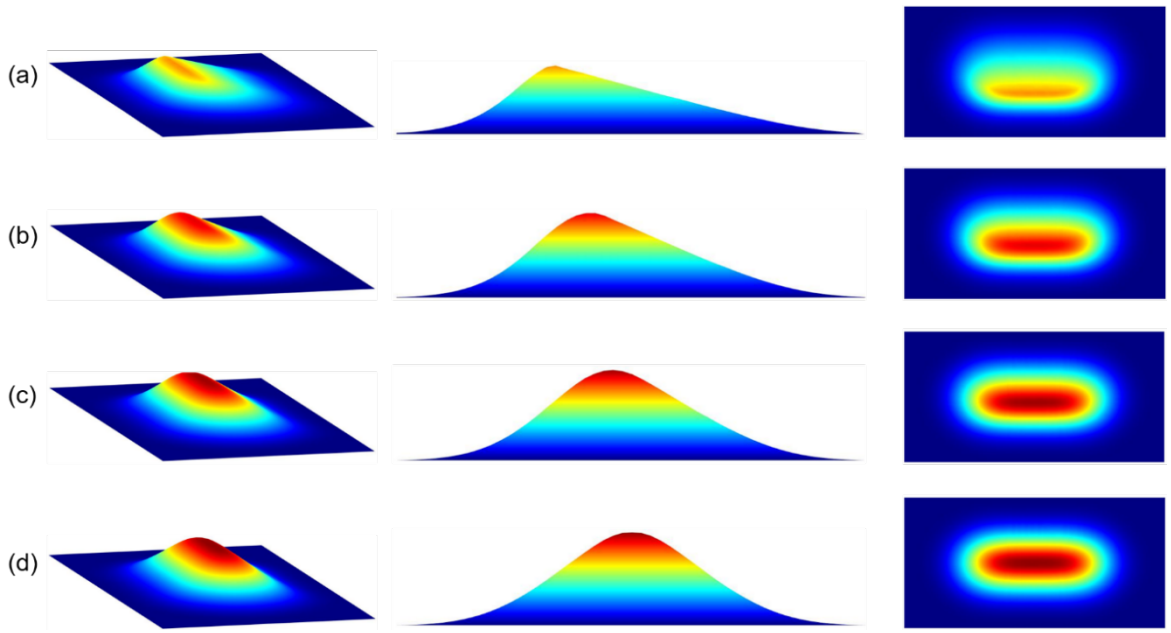


Figure 6 - 3D simulated isometric, front and top view profiles illustrating the effect of spray angle on the shape of deposits obtained by 20 passes for Ti6Al4V (a) Profiles corresponding to deposits at 60° spray angle (b) Profiles corresponding to deposits at 70° spray angle (c) Profiles corresponding to deposits at 80° spray angle (d) Profiles corresponding to deposits at 90° spray angle

3.3 The effect of scanning speed

In general, a good fitting was obtained when the model was used to analyze the effect of different scanning speeds, as demonstrated in Fig. 7 for Ti6Al4V. Variation of the scanning speed affects both the height of the deposit and its shape, but in a different way compared to their evolution in multiple passes. This variation happens as during deposition the profile of the target region where the particles impact changes. At each pass, a higher quantity of powder particles can be deposited at lower speeds. Therefore, keeping the number of scanning passes constant and using lower transverse speed will result in thicker deposits [24, 25, 31].

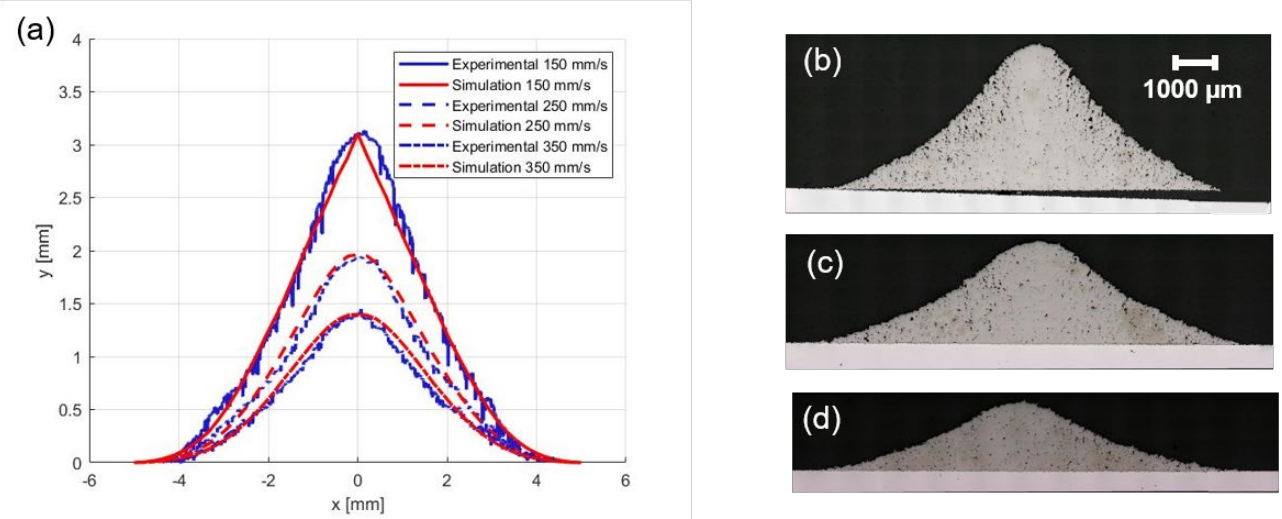


Figure 7 – The effect of scanning speed (a) Comparison of the simulation results with experimental data for Ti6Al4V sprayed at different scanning speeds (b) Cross-section of 20 passes deposit obtained at scanning speed of 150 mm/s (iii) Cross-section of 20 passes deposit obtained at scanning speed of 250 mm/s (iv) Cross-section of 20 passes deposit obtained at scanning speed of 350 mm/s.

Moreover, in the case of scanning speed, the RMSEs obtained by employing the present model was compared with the values obtained by Chen et al. [25] for Al5056 (with the model indicated as TST in table 1). The results are compared in Table 5. The data obtained from the model developed in this paper is found to be more accurate in simulating high transverse speed while it is slightly less accurate when lower speeds are used. On average, the new model leads to a lower value of RMSE and thus higher accuracy.

Table 7 – RMSE comparison between the prediction of different models for Al5056

Transverse Speed [mm/s]	**Present model normalized RMSE**	**Chen et al. [25] model normalized RMSE**
50	0.1311	0.1122
100	0.1548	0.1361
150	0.1518	0.1965
200	0.1648	0.2124
300	0.2208	0.2360

3.4 The effect of spray distance

The profiles obtained for Ti6Al4V for varying spray distances are shown in Fig. 8. The results indicate the strong dependency of deposit thickness on DE, which is in turn influenced by spray distance. The shape and width of the profile, on the other hand, mainly depend on particle jet dispersion; this dispersion, despite being relatively low, tends to generate wider tracks as the spray distance increases.

Generally, a good fit was obtained between the simulations and the experimental profiles, in particular, for what concerns the peak height, the track width and the shape at the extremities. As expected, both in experimental and simulated profiles, with increasing the spray distance the peak height decreased and the deposit width increased, as also reported by Ikeuchi et al. [23]. Previous studies on the effect of spray distance on the CS deposit profile considered only its effect on DE [19]; however, the present model considers its effects

also on deposit thickness, shape, and width; these features were implemented by applying the mass conservation principle explained in Subsection 2.2.1.

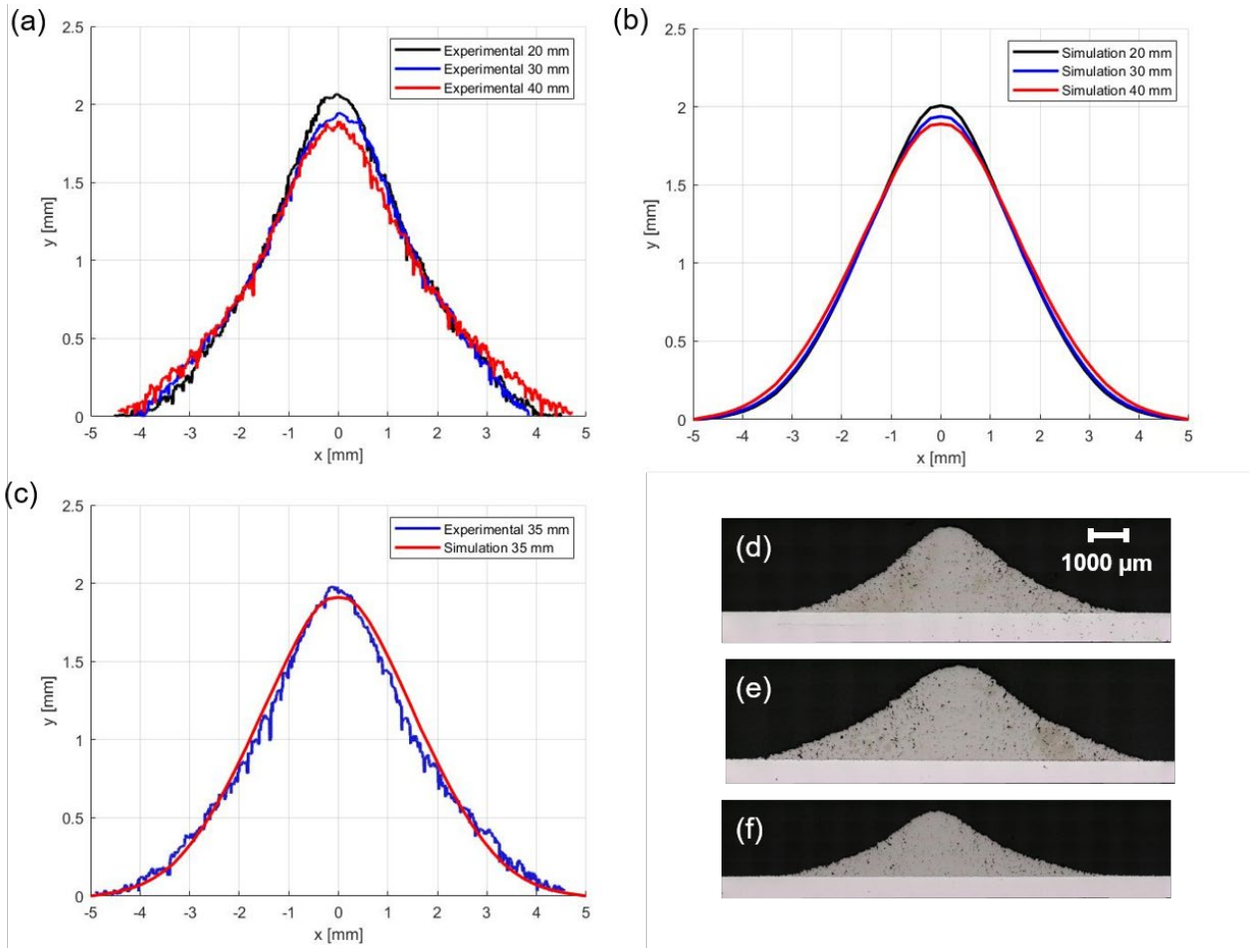


Figure 8 – The effect of spray distance on the shape of deposits of 20 passes Ti6Al4V (a) Experimental results for spray distance varying from 20 mm to 40 mm (b) Simulation results for spray distance varying from 20 mm to 40 mm (c) Comparison of experimental profile with simulation for spray distance of 35 mm as a representative profile among the predicted ones (d) Cross-section of deposit of 20 passes obtained with spray distance of 20 mm (e) Cross-section of deposit of 20 passes obtained with spray distance of 30 mm (e) Cross-section of deposit 20 passes obtained at spray distance 40 mm.

3.5 The effect of particle jet distribution

As already mentioned, Al2024 deposits exhibited a non-Gaussian particle jet distribution. A possible cause for this phenomenon could be the coarser powder PSD used in case of the aluminum alloy as described in Table 2. No literature data is available on the form of deposit profiles obtained for similar particle jet distribution. A specific function was generated according to the profile experimentally observed for the Al2024 deposits and implemented in the model.

A set of representative results (one example for each varying parameter) for Al2024 is shown in Fig. 9, Fig. 10, Fig. 11 and Figure 12. A very good agreement was obtained between the model prediction and the experimental results, despite the complexity of the shape, the roughness, and the asymmetry of some experimental profiles. In particular, a high precision was observed in simulating the evolution of the profile for different number of layers. The transition is shown in Fig. 10 where 10 and 25 passes are simulated. The transition from a rather smooth profile to a sharper one characterized by the two inflection points is obtained showing an almost perfect fit. The results demonstrated the accuracy and flexibility of the predictive model also for non-Gaussian profiles.

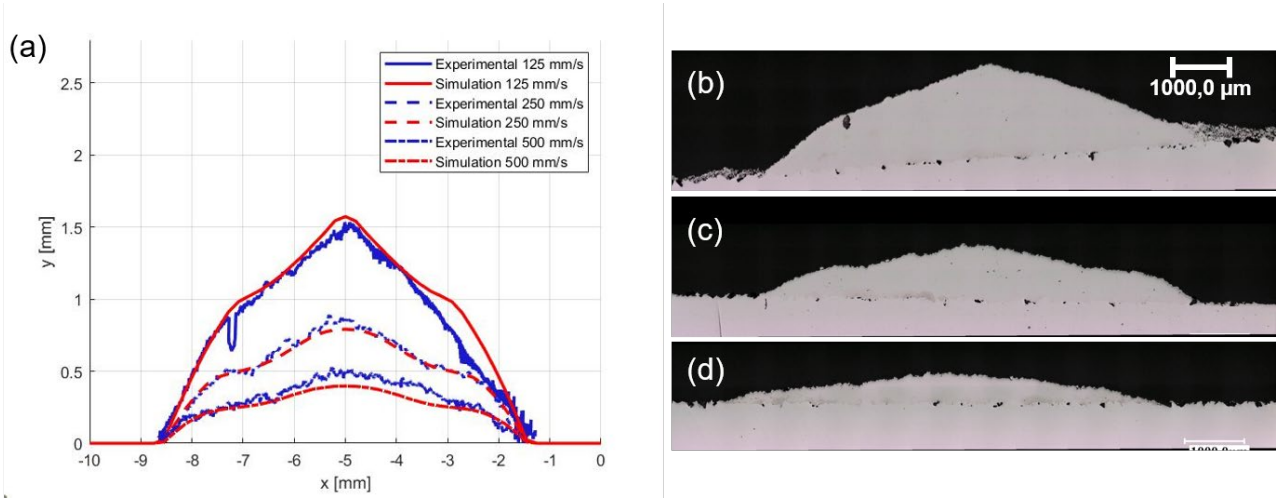


Figure 9 – Effect of scanning speed (a) Comparison of simulation results with experimental data for Al2024 sprayed at different scanning speeds (b) Cross-section of 10 passes deposited at scanning speed of 125 mm/s (c) Cross-section of 10 passes deposited at scanning speed of 250 mm/s (d) Cross-section of 10 passes deposited at scanning speed of 500 mm/s.

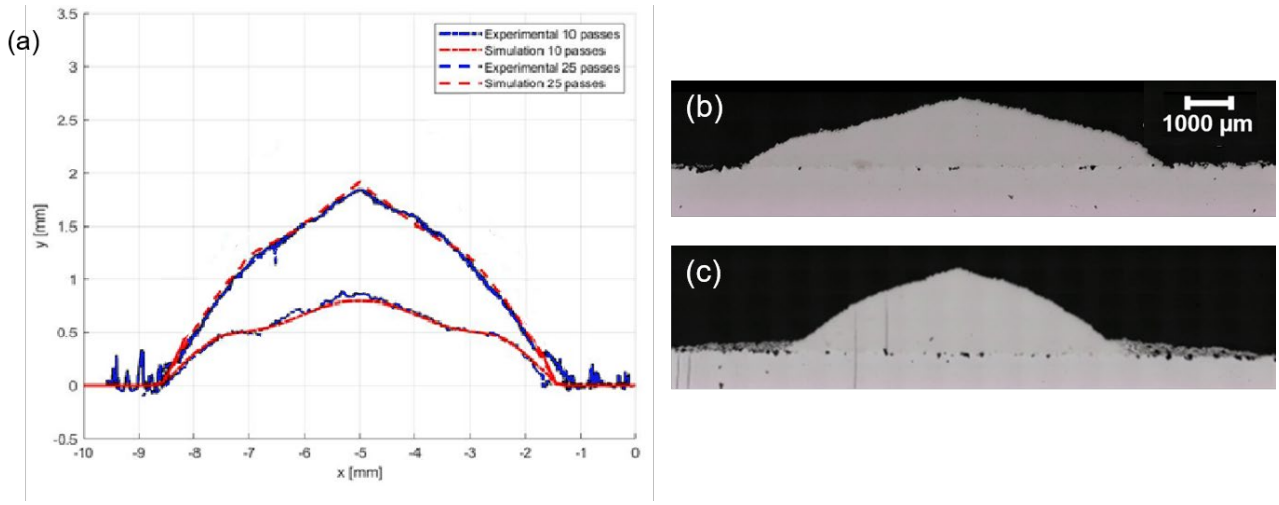


Figure 10 - The effect of number of scanning passes (a) Comparison of simulation results with the experimental profiles for Al2024 deposits obtained for 10 and 25 passes (b) Cross-section of Al2024 deposit with 10 passes (c) Cross section of Al2024 deposit with 25 passes

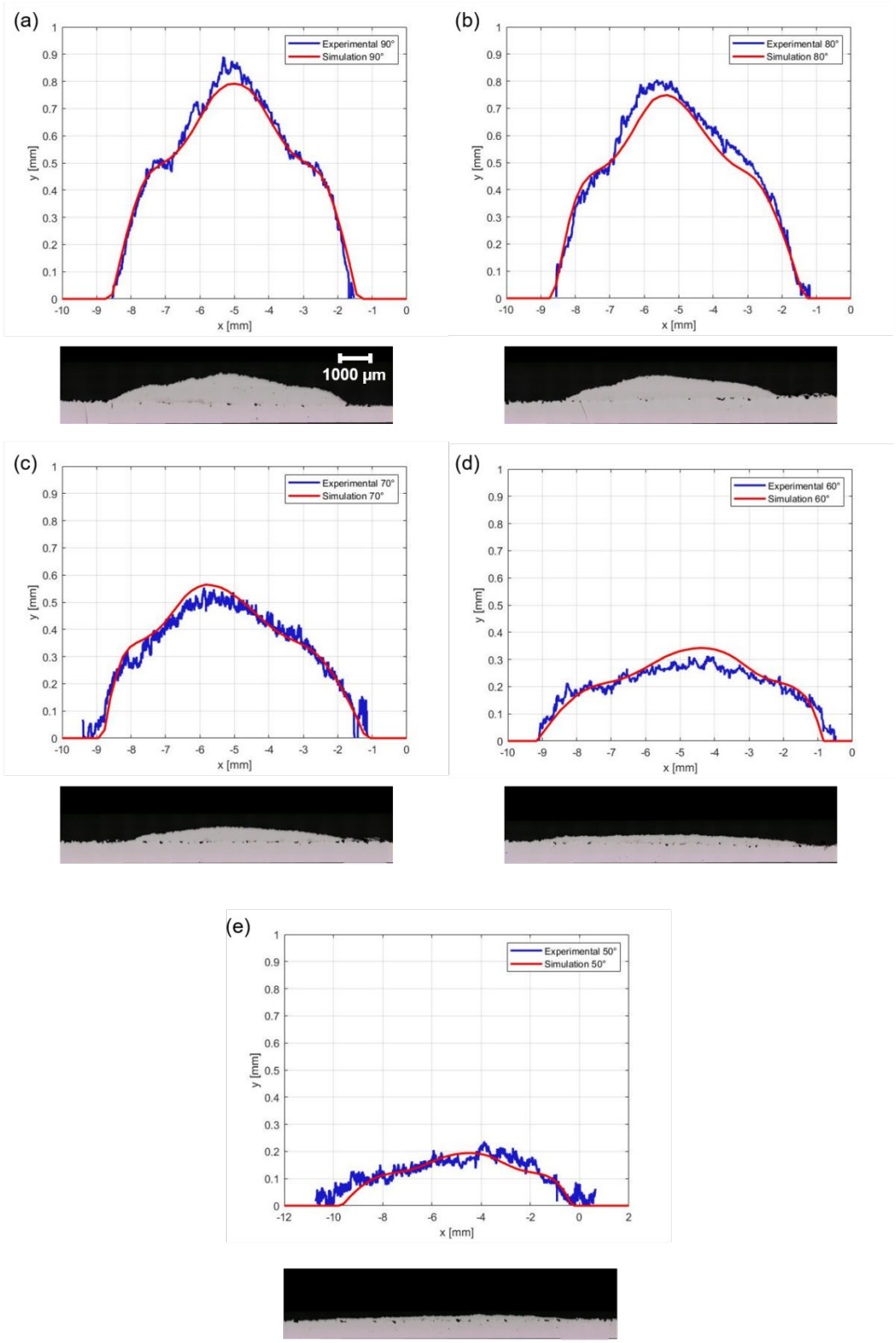


Figure 11 - The effect of spray angle on the shape of Al2024: comparison of simulation prediction and the experimental results together with the corresponding cross-sectional micrographs for (a) 10 passes deposited at 90° spray angle (b) 10 passes deposited at 80° spray angle (c) 10 passes deposited at 70° spray angle (d) 10 passes deposited at 60° spray angle (e) 10 passes deposited at 50° spray angle

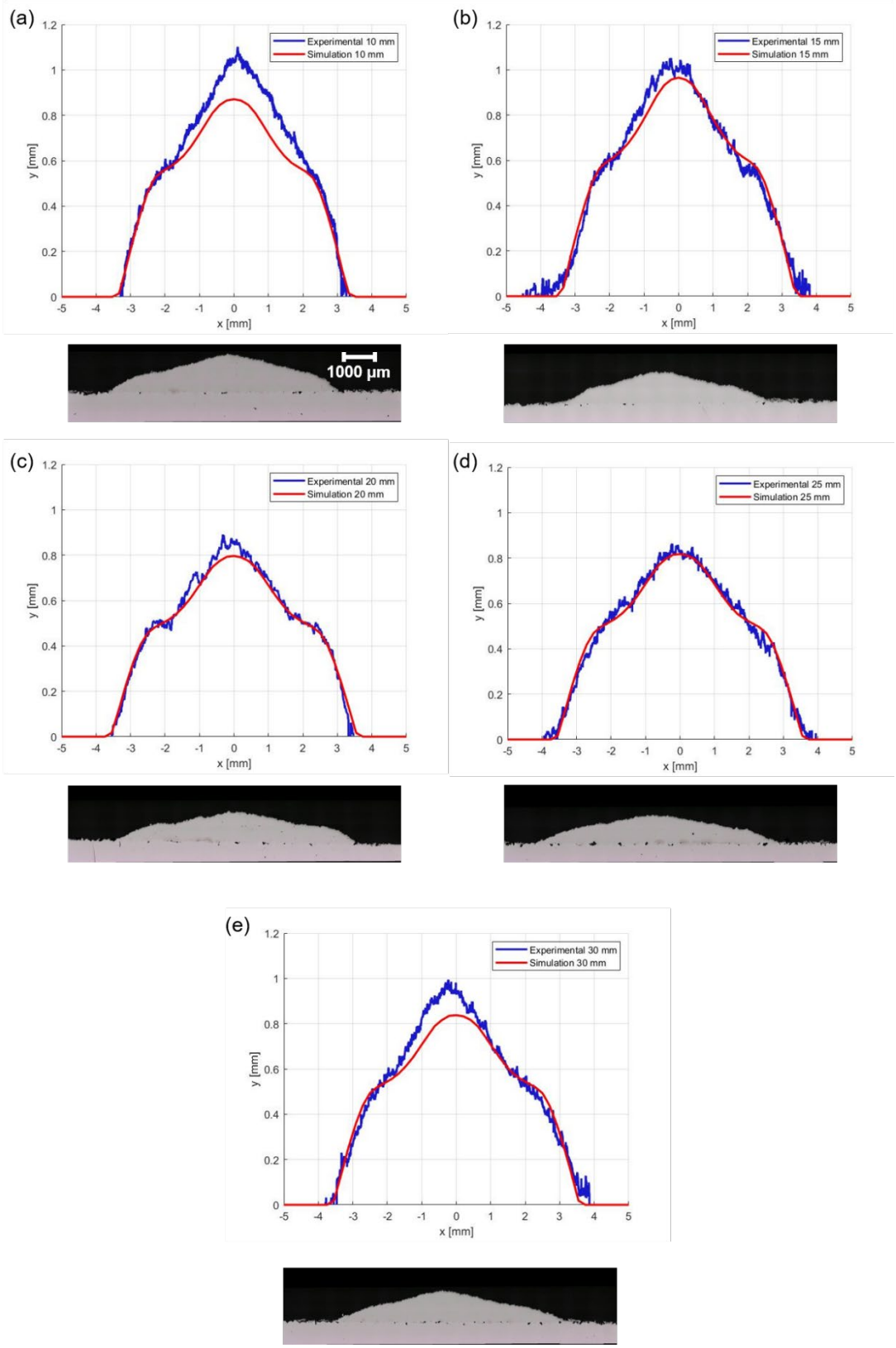


Figure 12 -The effect of spray distance on the shape of Al2024: comparison of simulation prediction and the experimental results together with the corresponding cross-sectional micrographs for (a) 10 passes deposited at 10 mm spray distance (b) 10 passes deposited at 15 mm spray distance (c) 10 passes deposited at 20 mm spray distance (d) 10 passes deposited at 25 mm spray distance (e) 10 passes deposited at 30 mm spray distance

3.6 Demonstrators

Superimposed tracks considering varied spray angles were simulated and compared with experimental profiles to demonstrate the capability of the developed model in predicting complex profiles and correctly mimicking the interaction between the previously deposited tracks and the newly deposited layers.

As the first case study we considered to implement the strategy suggested by Wu et al. [28], for spraying vertical walls, which the authors obtained with pure Cu. Given the results presented by Wu et al. [28], spraying a first track at 90° and a second one at 60° would lead to the formation of a plateau on top of the deposit for materials characterized with a Gaussian particle jet distribution. The expectations were met by both experimental and simulation results as it can be observed in the 2D section presented in Fig. 13a and in the 3D simulated profile represented in Fig. 13c. Very close fit was obtained with a value of normalized RMSE comparable to the ones obtained for single tracks. This implies that error propagation should not be necessarily expected when higher number of tracks are superimposed.

The second case study included spraying a single track on a curved substrate (a 42 mm diameter cylindrical surface) to assess the model capability in simulating the profile of deposits sprayed on non-planar substrates. Also, in this case, a good fit was obtained with only a slight underestimation of the profile peak height, as shown in Fig. 13b. Different views of the 3D profile shape are illustrated in Fig. 13d.

The last case study was designed with the aim of demonstrating the effectiveness of the model in simulating the shadow effect with a stepped-shape substrate sample. The result presented in Fig. 14b shows the 3D profile and demonstrates how the model is able to correctly identify the shadow regions and the areas where deposition occurs. In this case, due to predominant effect of fluid dynamics and the irregular profile of the sample, the simulation is able to reproduce the general shape, but it is not in catching the local features in the lower section of the profile as it can be noticed in Fig. 14d. However, the positive result regarding the identification of the shadow regions leads to the possibility to use the developed model on complex substrates where shadow effect is a fundamental prerequisite for the correctness of the simulation.

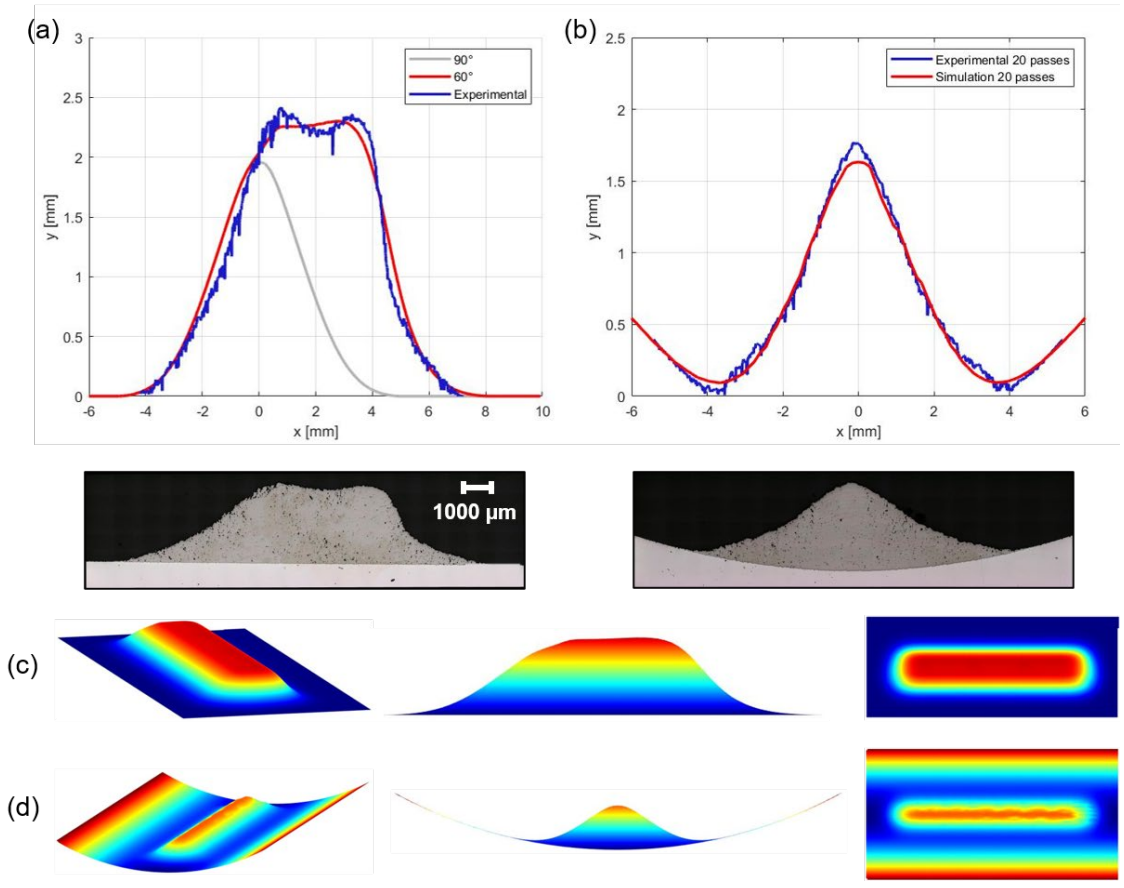


Figure 13 – Demonstrators: (a) Comparison of simulation results with experimental profiles for Ti6Al4V together with the corresponding cross-sectional micrographs for superimposed tracks (b) Comparison of simulation results with experimental profiles for Ti6Al4V together with the corresponding cross-sectional micrographs for single track on curved substrate (c) Isometric, front and top view 3D simulation profiles of superimposed tracks (b) Isometric, front and top view 3D simulation profiles of deposition on curved substrate

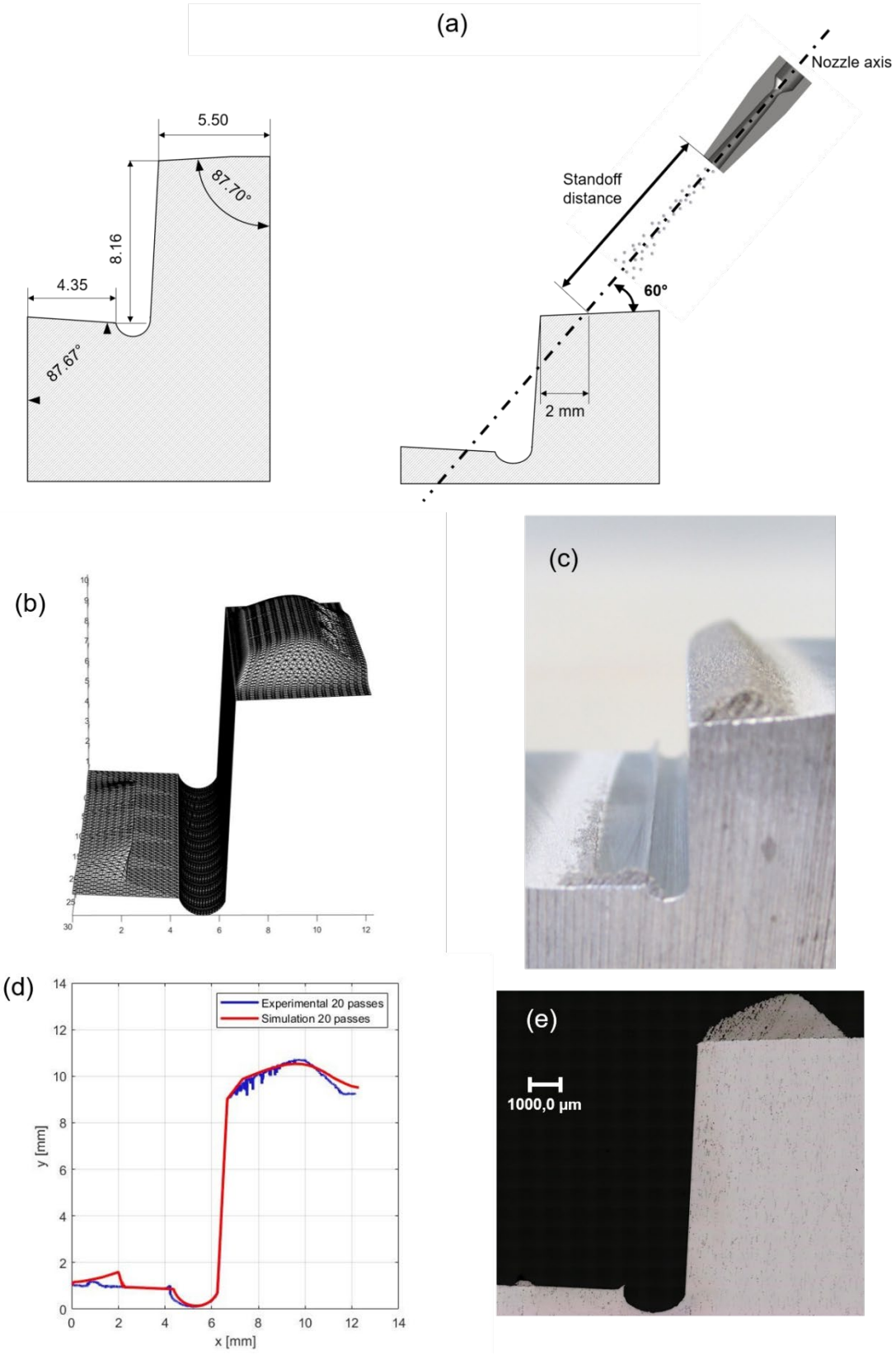


Figure 14 – Shadow effect: comparison of simulation results with experimental profiles for Ti6Al4V (a) Substrate geometry (b) 3D simulation profile (c) Experimental sample (d) Comparison of simulation results with experimental profiles for Ti6Al4V (e) Cross-section of 20 passes deposit

4. Critical considerations

The model's versatility was demonstrated by the high accuracy of predictions compared with the experimental profiles; however, some considerations have to be made regarding the limitations of the developed model.

An important aspect to be taken into account is associated with the definition of DE as a function of the impact angle. The DE curve that is used as an input for the model, is experimentally defined as a global parameter. Indeed, DE is typically calculated as the ratio between the weight of the sample before and after spraying and the mass of the sprayed powder. Furthermore, this measurement approach is inherently subjected to uncertainties. On the other hand, in the developed model, DE is considered locally since it is calculated for each single element face in the STL file. Therefore, the use of DE curves inside the model inevitably introduces a source of error, which can lead to a reduction of the accuracy especially in the case of low spray angles. An improvement in the DE measurement or the introduction of a method to obtain local DE values would thus further improve the simulation accuracy.

5. Conclusions

In this study, a 3D model was developed to predict the cold spray deposit profile. The simulation procedure was based on physical assumptions in line with the intrinsic features of cold spray deposition. The underlying physical principle consists of a partial differential equation describing the deposit growth and its shape evolution. The developed strategy was found to be more versatile with respect to the few existing models in terms of simulating the profile shape evolution and predicting the effect of various process parameters. Based on the obtained results the following conclusions can be drawn:

- This model offers a notable flexibility regarding the choice of the desired nozzle toolpath and substrate geometry.
- Single and multiple track deposits were considered for various materials. The developed model exhibits an accurate estimation of the deposit profile evolution as the number of passes increased.
- The model is able to simulate the effect of spray angle, scanning speed and spray distance on the profile shape regarding the deposit height, thickness, and peak position with a remarkable fidelity.
- The influence of all the analyzed parameters is successfully simulated in the case of the classical Gaussian as well as the non-Gaussian particle jet distribution profile.
- The model is validated also against experimental data for more complex case studies including superimposed tracks with different spray angles as well as single track on non-planar substrate, showing a very good match and stability.
- The developed model is able to simulate the shadow effect, showing a high potential to recognize when the formation of a deposit on a certain region of the substrate is hindered by the presence of other geometrical features.

Based on the detailed comparison of the model proposed in this manuscript and the already existing models for the shape prediction of cold spray profile, this new model provides a unique integrated solution to effectively simulate the cold spray deposit profile in complex conditions; the model is easily adaptable to a wide range of materials (with Gaussian or non-Gaussian particle jet distribution profile) and various shapes of substrates. The model was validated a broad range of different materials, namely, Cu, Al2024, Al5056, Al7075 and Ti6Al4V. The obtained results demonstrated the eminent robustness of the model and the possibility to apply it to a wide range of materials with distinctive properties and, thus, the opportunity to use it for different applications.

Therefore, the model will enable us to simulate the deposition profile both in the case of coatings and 3D near-net-shape components paving the way to industrial application of CSAM technology by enhancing its geometrical accuracy. Offering the possibility to accurately predict the shape of the deposit profile would be a step forward towards establishing cold spray as an additive manufacturing technique that can incorporate automatic generation of a toolpath, given the desired final geometry for complex shapes. The developed model would allow to quantify the deviation of the produced shape from the desired net-shape geometry. As future developments, the model could be integrated with the toolpath generation to turn it into a ready-to-use technology.

References

[1] H. Assadi, H. Kreye, F. Gärtner, T. Klassen, Cold spraying – A materials perspective, Acta Mater. 116 (2016) 382–407. https://doi.org/10.1016/j.actamat.2016.06.034.

[2] H. Singh, T.S. Sidhu, S.B.S. Kalsi, Cold spray technology: Future of coating deposition processes, Frat. Ed Integrita Strutt. 22 (2012) 69–84. https://doi.org/10.3221/IGF-ESIS.22.08.

[3] S. Yin, P. Cavaliere, B. Aldwell, R. Jenkins, H. Liao, W. Li, R. Lupoi, Cold spray additive manufacturing and repair: Fundamentals and applications, Addit. Manuf. 21 (2018) 628–650. https://doi.org/10.1016/j.addma.2018.04.017.

[4] R.N. Raoelison, Y. Xie, T. Sapanathan, M.P. Planche, R. Kromer, S. Costil, C. Langlade, Cold gas dynamic spray technology: A comprehensive review of processing conditions for various technological developments till to date, Addit. Manuf. 19 (2018) 134–159. https://doi.org/10.1016/j.addma.2017.07.001.

[5] F. Raletz, M. Vardelle, G. Ezo'o, Critical particle velocity under cold spray conditions, Surf. Coatings Technol. 201 (2006) 1942–1947. https://doi.org/10.1016/j.surfcoat.2006.04.061.

[6] H. Assadi, F. Gärtner, T. Stoltenhoff, H. Kreye, Bonding mechanism in cold gas spraying, Acta Mater. 51 (2003) 4379–4394. https://doi.org/10.1016/S1359-6454(03)00274-X.

[7] R. Ghelichi, S. Bagherifard, D. Mac Donald, M. Brochu, H. Jahed, B. Jodoin, M. Guagliano, Fatigue strength of Al alloy cold sprayed with nanocrystalline powders, Int. J. Fatigue. 65 (2014) 51–57. https://doi.org/10.1016/j.ijfatigue.2013.09.001.

[8] R. Ghelichi, D. MacDonald, S. Bagherifard, H. Jahed, M. Guagliano, B. Jodoin, Microstructure and fatigue behavior of cold spray coated Al5052, Acta Mater. 60 (2012) 6555–6561. https://doi.org/10.1016/j.actamat.2012.08.020.

[9] K. Petráčková, J. Kondás, M. Guagliano, Fixing a hole (with cold spray), Int. J. Fatigue. 110 (2018) 144–152. https://doi.org/10.1016/j.ijfatigue.2018.01.014.

[10] S. Bagherifard, M. Guagliano, Fatigue performance of cold spray deposits: Coating, repair and additive manufacturing cases, Int. J. Fatigue. 139 (2020) 105744. https://doi.org/10.1016/j.ijfatigue.2020.105744.

[11] W. Li, K. Yang, S. Yin, X. Yang, Y. Xu, R. Lupoi, Solid-state additive manufacturing and repairing by cold spraying: A review, J. Mater. Sci. Technol. 34 (2018) 440–457. https://doi.org/10.1016/j.jmst.2017.09.015.

[12] M.E. Lynch, W. Gu, T. El-Wardany, A. Hsu, D. Viens, A. Nardi, M. Klecka, Design and topology/shape structural optimisation for additively manufactured cold sprayed components: This paper presents an additive manufactured cold spray component which is shape optimised to achieve 60% reduction in stress and 20% reduction in weigh, Virtual Phys. Prototyp. 8 (2013) 213–231. https://doi.org/10.1080/17452759.2013.837629.

[13] S. Bagherifard, A. Heydari Astaraee, M. Locati, A. Nawaz, S. Monti, J. Kondás, R. Singh, M. Guagliano, Design and analysis of additive manufactured bimodal structures obtained by cold spray deposition, Addit. Manuf. 33 (2020). https://doi.org/10.1016/j.addma.2020.101131.

[14] T. Duda, L.V. Raghavan, 3D Metal Printing Technology, IFAC-PapersOnLine. 49 (2016) 103–110. https://doi.org/10.1016/j.ifacol.2016.11.111.

[15] A. Sova, S. Grigoriev, A. Okunkova, I. Smurov, Potential of cold gas dynamic spray as additive manufacturing technology, Int. J. Adv. Manuf. Technol. 69 (2013) 2269–2278. https://doi.org/10.1007/s00170-013-5166-8.

[16] R. Ghelichi, S. Bagherifard, D. Macdonald, I. Fernandez-Pariente, B. Jodoin, M. Guagliano, Experimental and numerical study of residual stress evolution in cold spray coating, Appl. Surf. Sci. 288 (2014) 26–33. https://doi.org/10.1016/j.apsusc.2013.09.074.

[17] S. Bagherifard, S. Monti, M.V. Zuccoli, M. Riccio, J. Kondás, M. Guagliano, Cold spray deposition for additive manufacturing of freeform structural components compared to selective laser melting, Mater. Sci. Eng. A. 721 (2018) 339–350. https://doi.org/10.1016/j.msea.2018.02.094.

[18] M. Vaezi, P. Drescher, H. Seitz, Beamless Metal Additive Manufacturing, Materials (Basel). 13 (2020). https://doi.org/10.3390/ma13040922.

[19] D. Ding, Z. Pan, D. Cuiuri, H. Li, A multi-bead overlapping model for robotic wire and arc additive manufacturing (WAAM), Robot. Comput. Integr. Manuf. 31 (2015) 101–110. https://doi.org/10.1016/j.rcim.2014.08.008.

[20] A.A. Ugla, O. Yilmaz, Deposition-Path Generation of SS308 Components Manufactured by TIG Welding-Based Shaped Metal Deposition Process, Arab. J. Sci. Eng. 42 (2017) 4701–4711.

https://doi.org/10.1007/s13369-017-2582-3.
[21] S. Saqiba, R.J. Urbanica, K. Aggarwal, Analysis of laser cladding bead morphology for developing additive manufacturing travel paths, Procedia CIRP. 17 (2014) 824–829. https://doi.org/10.1016/j.procir.2014.01.098.
[22] R. Liu, Z. Wang, Y. Zhang, T. Sparks, F. Liou, A smooth toolpath generation method for laser metal deposition, Solid Free. Fabr. 2016 Proc. 27th Annu. Int. Solid Free. Fabr. Symp. - An Addit. Manuf. Conf. SFF 2016. (2016) 1038–1046.
[23] D. Ikeuchi, A. Vargas-Uscategui, X. Wu, P.C. King, Neural network modelling of track profile in cold spray additive manufacturing, Materials (Basel). 12 (2019) 1–12. https://doi.org/10.3390/ma12172827.
[24] H. Wu, X. Xie, M. Liu, C. Chen, H. Liao, Y. Zhang, S. Deng, A new approach to simulate coating thickness in cold spray, Surf. Coatings Technol. 382 (2020) 125151. https://doi.org/10.1016/j.surfcoat.2019.125151.
[25] C. Chen, Y. Xie, C. Verdy, H. Liao, S. Deng, Modelling of coating thickness distribution and its application in offline programming software, Surf. Coatings Technol. 318 (2017) 315–325. https://doi.org/10.1016/j.surfcoat.2016.10.044.
[26] Z. Cai, S. Deng, H. Liao, C. Zeng, G. Montavon, The effect of spray distance and scanning step on the coating thickness uniformity in cold spray process, J. Therm. Spray Technol. 23 (2014) 354–362. https://doi.org/10.1007/s11666-013-0002-0.
[27] S. V. Klinkov, V.F. Kosarev, N.S. Ryashin, V.S. Shikalov, Influence of particle impact angle on formation of profile of single coating track during cold spraying, AIP Conf. Proc. 2027 (2018). https://doi.org/10.1063/1.5065085.
[28] H. Wu, X. Xie, M. Liu, C. Verdy, Y. Zhang, H. Liao, S. Deng, Stable layer-building strategy to enhance cold-spray-based additive manufacturing, Addit. Manuf. 35 (2020) 101356. https://doi.org/10.1016/j.addma.2020.101356.
[29] S. Pathak, G.C. Saha, Cold Spray in the Realm of Additive Manufacturing, 2020. http://link.springer.com/10.1007/978-3-030-42756-6.
[30] S. V. Klinkov, V.F. Kosarev, V.S. Shikalov, Control of cold spray process by changing of nozzle setting angle, AIP Conf. Proc. 2125 (2019). https://doi.org/10.1063/1.5117382.
[31] D. Kotoban, S. Grigoriev, A. Okunkova, A. Sova, Influence of a shape of single track on deposition efficiency of 316L stainless steel powder in cold spray, Surf. Coatings Technol. 309 (2017) 951–958. https://doi.org/10.1016/j.surfcoat.2016.10.052.
[32] S. V. Klinkov, V.F. Kosarev, V.S. Shikalov, Influence of nozzle velocity and powder feed rate on the coating mass and deposition efficiency in cold spraying, Surf. Coatings Technol. 367 (2019) 231–243. https://doi.org/10.1016/j.surfcoat.2019.04.004.
[33] S. Hamdi, W. Schiesser, G. Griffiths, Method of lines, Scholarpedia. 2 (2007) 2859. https://doi.org/10.4249/scholarpedia.2859.
[34] D.V. Griffiths, I.M. Smith, Numerical Methods for Engineers, Numer. Methods Eng. (2006). https://doi.org/10.1201/9781420010244.